A Coupled Atmosphere–Ocean Radiative Transfer System Using the Analytic Four-Stream Approximation

WEI-LIANG LEE AND K. N. LIOU

Department of Atmospheric and Oceanic Sciences, University of California, Los Angeles, Los Angeles, California

(Manuscript received 12 June 2006, in final form 13 December 2006)

ABSTRACT

A coupled atmosphere–ocean radiative transfer model based on the analytic four-stream approximation has been developed. It is shown that this radiation model is computationally efficient and at the same time can achieve acceptable accuracy for flux and heating rate calculations in the atmosphere and the oceans. To take into account the reflection and transmission of the wind-blown air–water interface, a Monte Carlo method has been employed to simulate the traveling of photons and to compute the reflectance and transmittance of direct and diffuse solar fluxes at the ocean surface. For the ocean part, existing bio-optical models, which correlate the concentration of chlorophyll and the absorption and scattering coefficients of phytoplankton and other matters, have been integrated into this coupled model. Comparing to the values computed by more discrete streams illustrates that the relative accuracies of the surface albedo and total transmission in the ocean determined from the present model are generally within 5%, except in cases of the solar zenith angle larger than 80°. Observational data have also been used to validate this model and the results show that the relative differences of downward and upward shortwave fluxes and albedo are within 10% of the observed values. This computationally efficient and physically based radiative transfer model is well suited for consistent flux calculations in a coupled atmosphere–ocean dynamic system.

1. Introduction

Energy transfer across the sea surface is crucial to the understanding of the general circulation of the ocean. Shortwave radiation from the sun contributes most of the heat fluxes that penetrate the air–sea interface and are subsequently absorbed throughout the ocean mixed layer. Solar radiative transfer differs from other air–sea interaction processes such as wind stress, evaporation, precipitation, and sensible cooling that occur only at the sea surface. Ohlmann et al. (1996) showed that the climatological value of solar flux penetrating the mixed layer can reach 40 W m^{-2} in the tropical regions and can produce a difference in the heating rate of a 20-m mixed layer by about 0.33°C a month. The vertical distribution of solar flux also influences the stability and stratification of the mixed layer and the sea surface temperature. It is clear that a quantitative understanding of the solar flux profile is important to ocean model simulations.

The surface albedo, which includes the surface reflectivity and the upwelling radiation from the water surface, is critical to the energy budget in the atmospheric planetary boundary layer. However, the reflectivity of the wind-blown surface is difficult to evaluate. Mobley (1994) showed that the surface reflectance may decrease by 50% when the solar zenith angle (SZA) is 70° and the wind speed increases from 0 to 20 m s^{-1}. The surface roughness also affects the upwelling radiation from the water surface and its determination requires accurate radiative transfer analysis. The impact of oceanic pigment on radiative transfer in the ocean is important, as discussed by Gordon et al. (1988) and Morel (1988). A change of 0.10 mg m^{-3} in the phytoplankton concentration in the mixed layer can result in a corresponding change of the penetrative solar flux by about 10 W m^{-2} at a level of 20-m depth (Siegel et al. 1995). Because solar radiation is the energy source for photosynthesis, it also directly affects the marine productivity.

The objective of this study is to build an efficient coupled ocean–atmosphere radiative transfer model in-

Corresponding author address: Wei-Liang Lee, Department of Atmospheric and Oceanic Sciences, University of California, Los Angeles, Los Angeles, CA 90095-1565.
E-mail: wllee@atmos.ucla.edu

DOI: 10.1175/JAS4004.1

cluding consideration of the wind-blown sea surface. At the present time, a typical coupled model either deals with radiative transfer in the atmosphere and ocean separately by considering one medium as the boundary condition for the other or is computationally expensive for solar flux calculation. The present coupled model is based on the delta-four-stream approximation, developed by Liou (1974) and Liou et al. (1988), that can provide an analytical solution for radiative flux calculation and at the same time maintain excellent accuracy. To include the effect of the wind-blown sea surface, a Monte Carlo method (see, e.g., Preisendorfer and Mobley 1985) that simulates the traveling of photons is employed to calculate the surface reflectance and transmittance. Applying the results from the Monte Carlo simulation into the delta-four-stream approximation, radiative transfer in the atmosphere and the ocean can be treated simultaneously and consistently. The present model is computationally efficient and provides a physically consistent surface albedo and ocean heating rate profile in the mixed layer.

In section 2, we first derive the solution of the four-stream approximation for a coupled atmosphere–ocean system, followed by a discussion of a Monte Carlo model that calculates the reflection and transmission functions of the wind-blown surfaces in section 2. Some model results are presented in section 3 and compared to those determined by a discrete-ordinates radiative transfer model. In section 4, we compare the model results to the observational data collected at the Clouds and the Earth's Radiant Energy System (CERES) Ocean Validation Experiment (COVE) site. Finally, conclusions are given in section 5.

2. Radiative transfer model

a. Four-stream approximation

In a homogeneous, plane-parallel media, the azimuth-independent radiative transfer equation governing the diffuse solar radiance I is given by (Chandrasekhar 1950; Liou 2002)

$$\mu \frac{dI(\tau, \mu)}{d\tau} = I(\tau, \mu) - \frac{\tilde{\omega}}{2} \int_{-1}^{1} I(\tau, \mu') P(\mu, \mu')\, d\mu' - Q_{a,s}(\tau, \mu), \quad (1)$$

where μ is the cosine of zenith angle θ, τ is the normal optical depth, $\tilde{\omega}$ is the single-scattering albedo, Q_a and Q_s are the direct solar components of the source term for the atmosphere and the sea, respectively, and the azimuthally averaged scattering phase function $P(\mu, \mu')$ can be expanded in terms of Legendre polynomial P_l in the form

$$P(\mu, \mu') = \frac{1}{2\pi} \int_0^{2\pi} P(\mu, \varphi; \mu', \varphi')\, d\varphi' = \sum_{l=0}^{N} \tilde{\omega}_l P_l(\mu) P_l(\mu'), \quad (2)$$

where $\tilde{\omega}_l$ is the expansion coefficient. In the atmospheric part, Q_a is the summation of downward and upward solar incident source terms and can be expressed as

$$Q_a(\tau, \mu) = \frac{\tilde{\omega} F_0}{4\pi} P(\mu, -\mu_0) e^{-\tau/\mu_0} + \frac{\tilde{\omega} F_0}{4\pi} e^{-\tau_A/\mu_0} \int_0^1 R(\mu'', -\mu_0) \times \left|\frac{\mu_0}{\mu''}\right| P(\mu, \mu'') e^{-(\tau_A - \tau)/\mu''}\, d\mu'', \quad (3a)$$

where F_0 is the direct solar flux at the top of the atmosphere, μ_0 is the cosine of the solar zenith angle (SZA) θ_0, τ_A is the total optical depth of the atmosphere, and $R(\mu'', -\mu_0)$ denotes the sea surface reflectance of the direct solar radiation originally traveling in the direction $-\mu_0$ and being reflected to the direction μ''. The first term on the right-hand side of Eq. (3a) represents the single scattering contribution of a direct downward solar beam, while the second term is the total contribution of an upward solar beam from various directions reflected by a wind-blown sea surface. For the oceanic part, only the downward direct solar radiation is considered so that the direct source term can be expressed as

$$Q_s(\tau, \mu) = \frac{\tilde{\omega} F_0}{4\pi} e^{-\tau_A/\mu_0} \int_{-1}^{0} T(-\mu'', -\mu_0) \times \left|\frac{\mu_0}{\mu''}\right| P(\mu, -\mu'') e^{-(\tau - \tau_A)/\mu''}\, d\mu'', \quad (3b)$$

where $T(-\mu'', -\mu_0)$ is the sea surface transmittance of the direct solar radiation from the direction $-\mu_0$ to the direction $-\mu''$.

Employing the Gauss formula, all the integrals in the preceding equations can be replaced by summations. Setting $I_i = I(\tau, \mu_i)$, Eq. (1) for the atmospheric part can be written as

$$\mu_i \frac{dI_i}{d\tau} = I_i - \frac{\tilde{\omega}}{2}\sum_{l=0}^{N}\tilde{\omega}_l P_l(\mu_i)\sum_{j=-n}^{n} a_j P_l(\mu_j) I_j - \frac{\tilde{\omega}F_0}{4\pi}\sum_{l=0}^{N}\tilde{\omega}_l P_l(\mu_i) P_l(-\mu_0) e^{-\tau/\mu_0} - \frac{\tilde{\omega}F_0}{4\pi} e^{-\tau_A/\mu_0}\sum_{l=0}^{N}\tilde{\omega}_l P_l(\mu_i)\sum_m R(\mu_m, -\mu_0) \times \left|\frac{\mu_0}{\mu_m}\right| P_l(\mu_m) e^{-(\tau_A-\tau)/\mu_m}, \quad i = \pm 1, \ldots, \pm n, \tag{4a}$$

where the Gauss quadrature points $\mu_j = -\mu_{-j}$, $j \neq 0$, and the weights $a_{-j} = a_j$, which satisfy $\Sigma_{j=-n}^{n} a_j = 2$. Correspondingly, Eq. (1) for the oceanic part is

$$\mu_i \frac{dI_i}{d\tau} = I_i - \frac{\tilde{\omega}}{2}\sum_{l=0}^{N}\tilde{\omega}_l P_l(\mu_i)\sum_{j=-n}^{n} a_j P_l(\mu_j) I_j - \frac{\tilde{\omega}F_0}{4\pi} e^{-\tau_A/\mu_0}\sum_{l=0}^{N}\tilde{\omega}_l P_l(\mu_i)\sum_m T(-\mu_m, -\mu_0) \times \left|\frac{\mu_0}{\mu_m}\right| P_l(\mu_m) e^{-(\tau-\tau_A)/\mu_m}, \quad i = \pm 1, \ldots, \pm n. \tag{4b}$$

In the four-stream approximation, two upward and two downward radiative streams are considered (i.e., $n = 2$), and at the same time the scattering phase function is expanded into four terms (i.e., $N = 3$). The following double Gauss quadratures and weights are used (Sykes 1951):

$$\begin{cases} \mu_1 = -\mu_{-1} = 0.2113248, & a_1 = a_{-1} = 0.5, \\ \mu_2 = -\mu_{-2} = 0.7886752, & a_2 = a_{-2} = 0.5. \end{cases} \tag{5}$$

Following the derivation given by Liou et al. (1988), the solution for the four-stream approximation for an atmospheric homogeneous layer can be written in the form

$$I_i = \sum_{j=1}^{2}\left[C_{i,j} G_i e^{-k_j\tau} + C_{i,-j} G_i e^{-k_j(\tau_1-\tau)}\right] + Z_i(-\mu_0) e^{-\tau/\mu_0} + e^{-\tau_A/\mu_0}\sum_m Z_i(\mu_m) \times \left|\frac{\mu_0}{\mu_m}\right| R(\mu_m, -\mu_0) e^{-(\tau_A-\tau)/\mu_m}, \quad i = \pm 1, \pm 2, \tag{6a}$$

where k_j and $C_{i,j}$ are the eigenvalues and eigenvectors, respectively, Z_i are particular solutions for the direct solar source term, and G_i are coefficients to be determined by the boundary conditions. Likewise, the solution for a homogeneous oceanic layer is given by

$$I_i = \sum_{j=1}^{2}\left[C_{i,j} G_i e^{-k_j\tau} + C_{i,-j} G_i e^{-k_j(\tau_1-\tau)}\right] + e^{-\tau_A/\mu_0}\sum_m Z_i(-\mu_m) \times \left|\frac{\mu_0}{\mu_m}\right| T(-\mu_m, -\mu_0) e^{-(\tau-\tau_A)/\mu_m}, \quad i = \pm 1, \pm 2. \tag{6b}$$

Figure 1 illustrates a coupled atmosphere–ocean system with the solar beam reflected and refracted by a wind-blown sea surface. For an optically inhomogeneous system, the atmosphere and ocean can be divided into L_1 and L_2 homogeneous layers, respectively. Each layer can be characterized by a single-scattering albedo, a scattering phase function, and an extinction coefficient. Therefore, we have $4 \times (L_1 + L_2)$ equations to determine $4 \times (L_1 + L_2)$ unknown coefficients.

The upward and downward intensities must be continuous at the interface of each adjacent layer in the atmosphere and the ocean. Except at the air–sea interface, the boundary conditions at the interfaces can be written as

$$I_i^{(l)}(\tau_l) = I_i^{(l+1)}(\tau_l), \quad i = \pm 1, \pm 2, \tag{7}$$

where $I^{(l)}$ represents the radiative intensities in layer l, and τ_l is the optical depth from the top of the atmosphere to the bottom of the l layer. At the top of the atmosphere we assume that there is no downward diffuse solar radiance, so

$$I_{-1,-2}(\tau = 0) = 0. \tag{8}$$

At the bottom of the ocean, the Lambertian surface is assumed. Let the albedo of the ocean bottom be r_s and the total optical depth of the ocean be τ_s; then the upward diffuse radiances reflected from the ocean bottom can be expressed by

$$I_{1,2}^{(L_1+L_2)}(\tau_{L_1+L_2}) = \frac{r_s}{\pi}\left[2\pi(a_1\mu_1 I_{-1} + a_2\mu_2 I_{-2}) + e^{-\tau_A/\mu_0}\sum_m \mu_m F_0 e^{-\tau_s/\mu_m}\right]. \tag{9}$$

For the determination of the boundary conditions at the air–sea interface, the upward diffuse intensities just above the sea surface can be represented by

$$I_i^{(L_1)}(\tau_{L_1}) = \sum_{j=1}^{2}\left[\overline{R}_{i,-j} I_{-j}^{(L_1)}(\tau_{L_1}) + \overline{T}_{i,j} I_j^{(L_1+1)}(\tau_{L_1})\right], \quad i = 1, 2, \tag{10a}$$

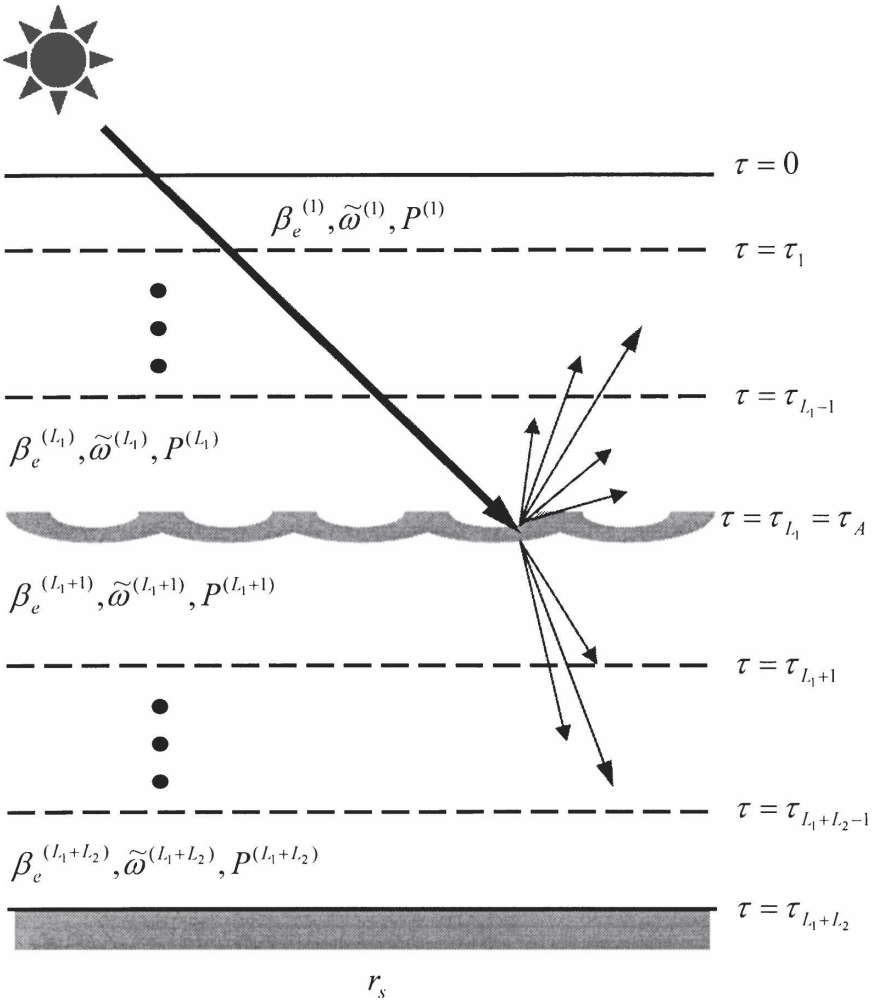

FIG. 1. Illustration of an inhomogeneous coupled atmosphere–ocean system. The atmosphere and ocean are divided into L_1 and L_2 homogeneous layers, respectively.

where $\overline{R}_{i,-j}$ denotes the surface reflectance of the diffuse radiances from the direction μ_{-j} to μ_i and $\overline{T}_{i,j}$ denotes the surface transmittance of diffuse radiances from the direction μ_j to μ_i. The corresponding downward diffuse intensities just below the sea surface can be expressed by

$$I_{-i}^{(L_1+1)}(\tau_{L_1}) = \sum_{j=1}^{2} [\overline{T}_{-i,-j} I_{-j}^{(L_1)}(\tau_{L_1}) + \overline{R}_{-i,j} I_j^{(L_1+1)}(\tau_{L_1})], \quad i = 1, 2. \tag{10b}$$

Because there are two upward and two downward radiances to estimate the total diffuse radiation flux in the context of four-stream approximation, we partition both upper and lower hemispheres into two subdomains, such as Ω_2 ($1 \le \mu < 0.5$), Ω_1 ($0.5 \le \mu < 0$), Ω_{-1} ($0 < \mu \le -0.5$), and Ω_{-2} ($-0.5 < \mu \le 1$). Then the surface reflectance for diffuse radiation can be defined by

$$\overline{R}_{i,-j} = \left|\frac{\mu_{-j}}{\mu_i}\right| \frac{\int_{\mu=c_i}^{\mu=c_i+0.5} \int_{\mu'=c_{-j}}^{\mu'=c_{-j}+0.5} R(\mu, -\mu')\, d\mu\, d\mu'}{\int_{\mu=c_i}^{\mu=c_i+0.5} \int_{\mu'=c_{-j}}^{\mu'=c_{-j}+0.5} d\mu\, d\mu'}, \quad i, j = \pm 1, \pm 2, \tag{11a}$$

where the lower limits of the integral are $c_2 = 0.5$, $c_1 = 0$, $c_{-1} = -0.5$, and $c_{-2} = -1$. Equation (11a) indicates that $\overline{R}_{i,-j}$ is a domain-averaged reflectance of all incident rays with directions in Ω_{-j} and the reflected rays with directions in Ω_i. The surface transmittance for diffuse radiation can also be defined by

$$\overline{T}_{i,j} = \left|\frac{\mu_j}{\mu_i}\right| \frac{\int_{\mu=c_i}^{\mu=c_i+0.5} \int_{\mu'=c_j}^{\mu'=c_j+0.5} T(\mu, \mu')\, d\mu\, d\mu'}{\int_{\mu=c_i}^{\mu=c_i+0.5} \int_{\mu'=c_j}^{\mu'=c_j+0.5} d\mu\, d\mu'},$$

$$i, j = \pm 1, \pm 2. \tag{11b}$$

The reflectance $\overline{R}_{i,-j}$ and transmittance $\overline{T}_{i,j}$ for diffuse radiation, as well as $R(\mu_m, -\mu_0)$ and $T(-\mu_m, -\mu_0)$ for direct solar beam, are computed by using the offline Monte Carlo simulation to be discussed below.

After all intensities are obtained, the total upward and downward fluxes for the atmospheric part at a given level l and optical depth τ are given by

$$F^{\uparrow}_{(l)}(\tau) = 2\pi[a_1\mu_1 I^{(l)}_1(\tau) + a_2\mu_2 I^{(l)}_2(\tau)] + F_0 e^{-\tau_A/\mu_0} \sum_m R(\mu_m, -\mu_0)\left|\frac{\mu_0}{\mu_m}\right| e^{-(\tau_A-\tau)/\mu_m},$$

$$F^{\downarrow}_{(l)}(\tau) = 2\pi[a_1\mu_1 I^{(l)}_{-1}(\tau) + a_2\mu_2 I^{(l)}_{-2}(\tau)] + \mu_0 F_0 e^{-\tau/\mu_0}. \tag{12a}$$

Correspondingly, the total upward and downward fluxes for the oceanic counterpart part are

$$F^{\uparrow}_{(l)}(\tau) = 2\pi[a_1\mu_1 I^{(l)}_1(\tau) + a_2\mu_2 I^{(l)}_2(\tau)],$$

$$F^{\downarrow}_{(l)}(\tau) = 2\pi[a_1\mu_1 I^{(l)}_{-1}(\tau) + a_2\mu_2 I^{(l)}_{-2}(\tau)] + F_0 e^{-\tau_A/\mu_0} \sum_m T(-\mu_m, -\mu_0)\left|\frac{\mu_0}{\mu_m}\right| e^{-(\tau-\tau_A)/\mu_m}. \tag{12b}$$

To account for the forward diffraction peak contribution in multiple scattering, we have incorporated the δ-function adjustment into the four-stream approximation. In this adjustment, the optical depth, the single-scattering albedo, and the expansion coefficients of the phase function can be redefined as follows (Liou et al. 1988):

$$\tau' = \tau(1 - f\tilde{\omega}),$$

$$\tilde{\omega}' = (1 - f)\tilde{\omega}/(1 - f\tilde{\omega}),$$

$$\tilde{\omega}'_l = [\tilde{\omega}_l - f(2l + 1)]/(1 - f), \quad l = 1, 2, 3, \tag{13}$$

where the fraction of the scattered energy residing in the forward peak $f = \tilde{\omega}_4/9$.

b. Radiative transfer across the air–sea interface

Change in the index of refraction across the air–water interface causes difficulties in radiative transfer calculations, particularly when the wind-blown sea surface is considered. To statistically estimate the reflectance and transmittance of diffuse and direct solar radiation, we employ the Monte Carlo method introduced by Preisendorfer and Mobley (1985) to construct a random wind-blown sea surface and to trace the interacting light rays.

Cox and Munk (1954) analyzed light reflection measurements from a wavy sea surface and derived a parameterization for the distribution of wave slopes such that the mean is equal to zero and the variance is proportional to the wind speed as follows:

$$\sigma_u^2 = 3.16 \times 10^{-3} \times U,$$

$$\sigma_c^2 = 1.92 \times 10^{-3} \times U + 0.03, \tag{14}$$

where U is the wind speed in m s^{-1} at a height 12.5 m mean sea level (MSL), and σ_u and σ_c are the standard deviations of wave slope distributions in the upwind and crosswind directions, respectively. A random wind-blown surface is partitioned into triangular facets over a hexagonal grid, while the slope distribution of the facets obeys the law described in Eq. (14). The directions and energies of the reflected and refracted rays are determined by Snell's law and Fresnel's formula, respectively. To account for strong absorption due to water in the infrared region, the generalized forms of Snell's law and Fresnel's formula for unpolarized light were used in the simulation and are respectively given by (Born and Wolf 1980)

$$\begin{cases} \sin\theta_i = N_w \sin\theta_t, & \text{for air-incident case} \\ N_w \sin\theta_i = \sin\theta_t, & \text{for water-incident case} \end{cases} \tag{15}$$

and

$$f_r = \frac{1}{2} f_i \left\{ \left[\frac{\sin(\theta_i - \theta_t)}{\sin(\theta_i + \theta_t)}\right]^2 + \left[\frac{\tan(\theta_i - \theta_t)}{\tan(\theta_i + \theta_t)}\right]^2 \right\}, \tag{16a}$$

$$f_t = f_i - f_r, \tag{16b}$$

where θ_i is the incident angle, θ_t is the transmitted angle, f_i is the incident flux, f_r is the reflected flux, f_t is the transmitted flux, and N_w is the adjusted real index of refraction of water defined by

$$N_w = \frac{\sqrt{2}}{2}\{m_r^2 - m_i^2 + \sin^2\theta_i + [(m_r^2 - m_i^2 - \sin^2\theta_i)^2 + 4m_r^2 m_i^2]^{1/2}\}^{1/2}, \tag{17}$$

where m_r and m_i are the real and imaginary refractive indices of water, respectively.

Whitecaps and foam may contribute to the reflectance of the sea surface. However, Moore et al. (2000) found that whitecaps increase the reflectance in the visible region only by 0.001–0.002 in the Tropics when the

wind speed ranges from 9 to 12 m s^{-1}, which is less than 7% of the Fresnel reflectance using the same wind speed. Furthermore, Frouin et al. (1996) and Moore et al. (2000) showed that the reflectance of whitecaps decreases significantly as wavelength increases in the near-infrared region. For these reasons, we have neglected the effect of whitecaps and foam on sea surface albedo in the Monte Carlo simulation.

c. Model input

In this radiative transfer model, the solar and thermal IR regions are divided into 6 and 12 bands, respectively (Fu and Liou 1993). The spectral divisions for the solar region are 200–700, 700–1300, 1300–1900, 1900–2500, 2500–3500, and 3500–5000 nm. In the solar spectrum, we consider absorption due to H_2O, O_3, CO_2, and O_2. For nongray gaseous absorption, the correlated k-distribution (CKD) method developed by Fu and Liou (1992) is employed. Instead of the tedious line-by-line integration in the frequency domain (ν), the CKD uses the cumulative probability (g) of the absorption coefficient (k_ν) in a spectral interval ($\Delta\nu$) as an independent variable. This method significantly reduces computer time costs for spectral integration. Parameterization of the radiative properties of aerosols follows the scheme developed by Gu et al. (2003) for application to the University of California, Los Angeles (UCLA) GCM. Rayleigh scattering is also accounted for in the radiative transfer calculation. Clouds in the atmosphere can also be accounted for in this model if their single-scattering properties are given.

The spectral absorption coefficients of pure seawater between 200 and 800 nm are taken from Smith and Baker (1981), while the absorption beyond 800 nm is calculated from the imaginary part of the refractive index for pure water given by Hale and Querry (1973). Absorption by dissolved yellow matter is generally correlated to that by phytoplankton. Moreover, absorption due to the case 1 waters between 400 and 700 nm can be calculated using the bio-optical model developed by Morel and Maritorena (2001). The case 1 waters are in reference to phytoplankton and associated living or nonliving derivatives that are optically more important than nonbiogenic particles (Morel and Prieur 1977). Based on these considerations, the spectral absorption coefficient for yellow matter $a_y(\lambda)$ and the total spectral absorption coefficient $a(\lambda)$ can be expressed in terms of chlorophyll concentration in the forms

$$a_y(440) = 0.2\{a_w(440) + 0.06A_{\text{chl}}(440)[\text{chl}]^{0.65}\}, \quad (18a)$$

$$a_y(\lambda) = a_y(440)\exp[-0.014(\lambda - 440)], \quad (18b)$$

$$a(\lambda) = a_w(\lambda) + 0.06A_{\text{chl}}(\lambda)[\text{chl}]^{0.65} + a_y(\lambda), \quad (18c)$$

where [chl] is the chlorophyll concentration expressed in mg m^{-3}, $a_w(\lambda)$ is the absorption coefficient of pure seawater, $A_{\text{chl}}(\lambda)$ is a nondimensional statistically derived chlorophyll-specific absorption coefficient (Prieur and Sathyendranath 1981), $A_{\text{chl}}(440)$ is unity, and λ is in units of nanometers. Between 200 and 400 nm, the value of $A_{\text{chl}}(\lambda)$ is determined by linear extrapolation. For wavelengths greater than 700 nm, only pure water absorption is taken into account because the absorption due to phytoplankton and dissolved matter is weak (Morel 1991).

Rayleigh scattering theory is not applicable to water because the distance between water molecules in liquid phase is too short. The Einstein–Smoluchowski theory of scattering (Mobley 1994) states that fluctuation in the molecular number density due to random molecular motions causes fluctuation in the index of refraction, which gives rise to scattering. The net effect is that the volume scattering function for pure water is in the form

$$\beta_w(\theta, \lambda) = \beta_w(90^\circ, \lambda_0)\left(\frac{\lambda_0}{\lambda}\right)^{4.32}(1 + 0.835\cos^2\theta), \quad (19)$$

where λ_0 is the reference wavelength and θ is the scattering angle. The scattering coefficients between 200 and 800 nm for pure seawater, $b_w(\lambda)$, are taken from Smith and Baker (1981) and the values are extrapolated for wavelengths greater than 800 nm using the $\lambda^{-4.32}$ relationship denoted in Eq. (19). To determine the particulate scattering coefficient $b_p(\lambda)$, we employ the bio-optical model for scattering in case 1 waters developed by Gordon and Morel (1983) and modified by Morel and Maritorena (2001):

$$b_p(\lambda) = \left(\frac{550}{\lambda}\right)0.416[\text{chl}]^{0.766}. \quad (20)$$

The scattering phase function for natural seawater is the average of those from pure water and particulate weighted by the scattering coefficients of pure water and particulate, respectively, such that

$$P_s(\lambda) = \frac{b_w(\lambda)P_w + b_p(\lambda)P_p}{b_w(\lambda) + b_p(\lambda)}, \quad (21a)$$

where the particulate phase function P_p used follows the measurements made by Petzold (1972), while that for pure seawater P_w is given by [also see Eq. (19)]

$$P_w(\theta) = 0.782(1 + 0.835\cos^2\theta). \quad (21b)$$

In each Monte Carlo simulation, 50 000 wind-blown surfaces have been constructed for a given wind speed. There are 20 initial rays with unit power and a given direction assigned for each randomly constructed sur-

face consisting of 384 triangular facets in a hexagonal domain. Then the surface reflectance $R(\mu_m, -\mu_0)$ and transmittance $T(-\mu_m, -\mu_0)$ for direct solar radiation are calculated from the Monte Carlo simulation for wind speeds from 0 to 20 m s^{-1} with an interval of 1 m s^{-1} and SZA from 0° to 89° with an interval of 1°. It is followed by the construction of lookup tables for $R(\mu_m, -\mu_0)$, $T(-\mu_m, -\mu_0)$, $\overline{R}_{i,-j}$, and $\overline{T}_{i,j}$. Values for other angles can be computed by linear interpolation. For the case with the wind speed greater than 20 m s^{-1}, the reflectance and transmittance are determined by linear extrapolation.

Figure 2 shows the distribution of the reflected and transmitted intensity with the 20 m s^{-1} wind speed and different incident zenith angles. In the air-incident case of $\theta = 150°$ (upper panel), the scattering effect due to surface roughness on the reflected intensities is more pronounced than for the transmitted intensities. Total reflectance and transmittance are 0.0231 and 0.9769, respectively. Deviation due to surface roughness is about 1% as compared to the reflectance of 0.0229 for a flat surface. In the water-incident case of $\theta = 70°$, a small portion (0.14%) of radiant energy can escape from water, while it will encounter total internal reflection with a flat surface; that is, the transmittance is zero.

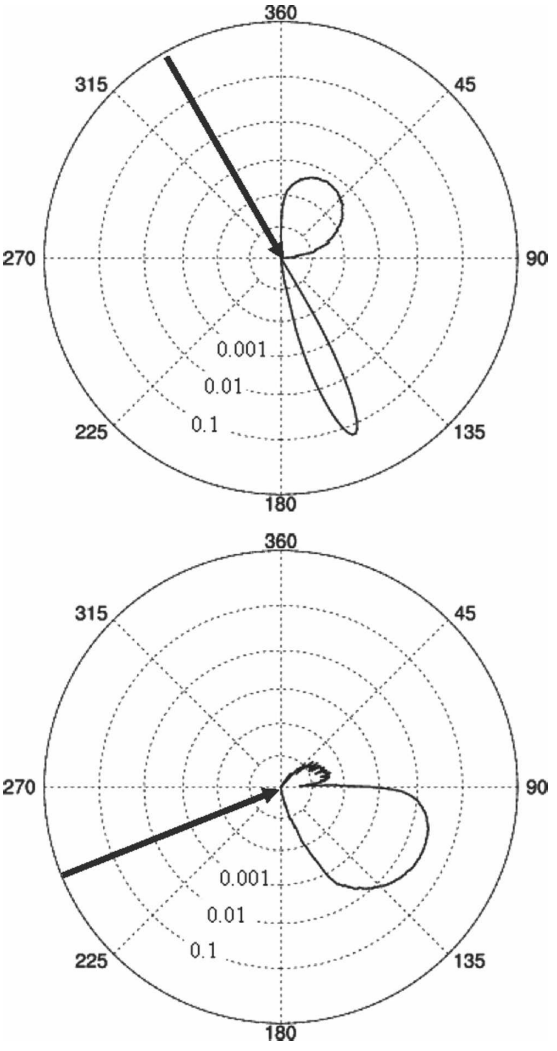

FIG. 2. Angular distribution of reflected and transmitted radiant power calculated by the Monte Carlo simulation. The circles indicate the scale for the fraction of incident energy that is transferred to various directions. The wind speed is 20 m s^{-1}, and the incident zenith angles are (upper) 150° and (lower) 70°, denoted by the thick arrows.

3. Model results

Using the radiative transfer scheme built in section 2, we compute the surface albedo α and transmission $T(z)$ for solar radiation defined in the form

$$\alpha = F_u(0^+)/F_d(0^+),$$
$$T(z) = F_d(z)/F_d(0^+), \quad (22)$$

where $F_u(0^+)$ and $F_d(0^+)$ are the total upward and downward fluxes just above the sea surface (0^+), respectively, and z is the depth of the ocean. An ocean depth of 200 m with an ocean bottom albedo of 0.1 is arbitrarily selected, and the chlorophyll concentration is considered uniform in the whole layer. Figure 3a shows the surface solar albedo as a function of the wind speed and the cosine of SZA for a clear-sky condition with chlorophyll concentrations of 0 and 12 mg m^{-3}. Sea surface albedo generally increases with SZA for $\mu_0 > 0.1$ because the Fresnel reflectance increases with increasing incident angle. However, the surface albedo decreases with SZA for $\mu_0 < 0.1$. This is because when the sun's altitude becomes lower, the intensity of direct solar radiation decreases more rapidly compared to that of diffuse radiation. Thus, the addition of the proportion of diffuse radiation reduces the effective SZA, leading to a decrease in surface albedo. The wind effect on the surface albedo is strong only when the sun is low. For air-incident rays, the Fresnel reflectance is almost constant for $\theta_0 < 50°$ and increases rapidly for $\theta_0 > 50°$. Thus, the wind-blown surface does not significantly change the surface albedo for $\mu_0 > 0.4$. It is noted that the surface albedo increases with chlorophyll concentration due to increase in the scattering coefficient. However, this effect is not significant because the increase in backscattering is canceled out by the increase in the particulate absorption in seawater.

Figure 3b shows the transmission $T(z = 5\text{ m})$ using chlorophyll concentrations of 0 and 2 mg m^{-3}. It is clear that the transmission decreases significantly with in-

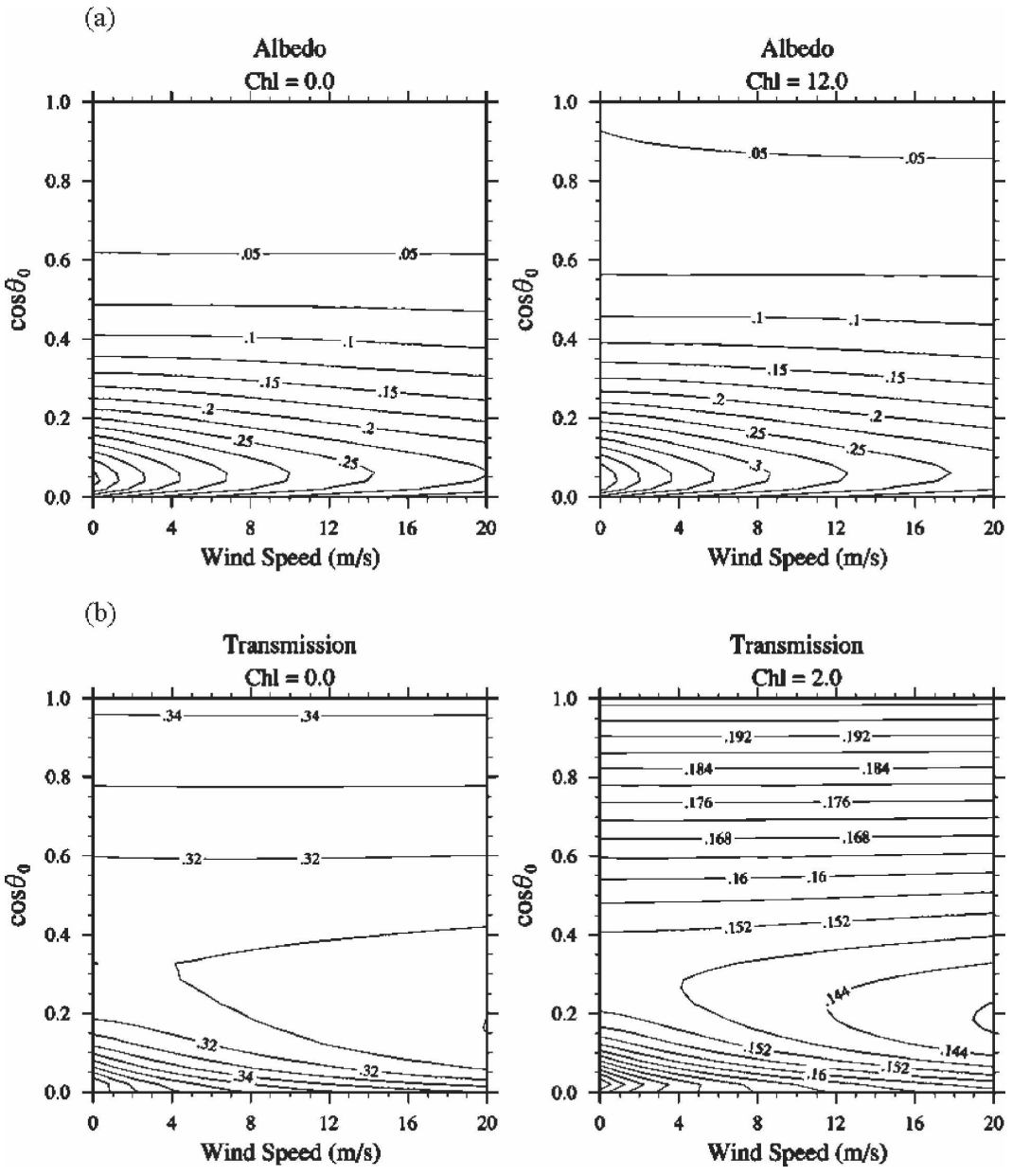

FIG. 3. (a) Sea surface albedo for radiation between 0.2 and 4.0 μm as a function of wind speed and cos(SZA) for the clear-sky condition with chlorophyll concentrations of (left) 0 and (right) 12 mg m^{-3}. (b) Transmission at ocean depth at 5 m with chlorophyll concentrations of (left) 0 and (right) 2 mg m^{-3}.

crease in chlorophyll concentration due to the increase in absorption. Note that the transmission minimum occurs at $\mu_0 \sim 0.25$. Because of Rayleigh scattering, the intensity in the blue light region of direct solar radiation decreases with increase in optical depth. Note that seawater has a minimum absorption coefficient in the blue light region; therefore, the transmission decreases with increasing SZA. However, there is more radiant intensity in the blue light region for diffuse radiation than direct radiation. Consequently, when the sun's altitude is very low, having more energy for diffuse radiation (relative to total incident radiation), the transmission increases with SZA.

The accuracy of this radiative transfer model is examined by comparing the model results to the values calculated by the Coupled Ocean–Atmosphere Radiative Transfer (COART) model (Jin and Stamnes 1994; Jin et al. 2002), which is also based on the discrete-ordinates method. In COART, 12 and 20 radiation streams are used for the atmosphere and the ocean,

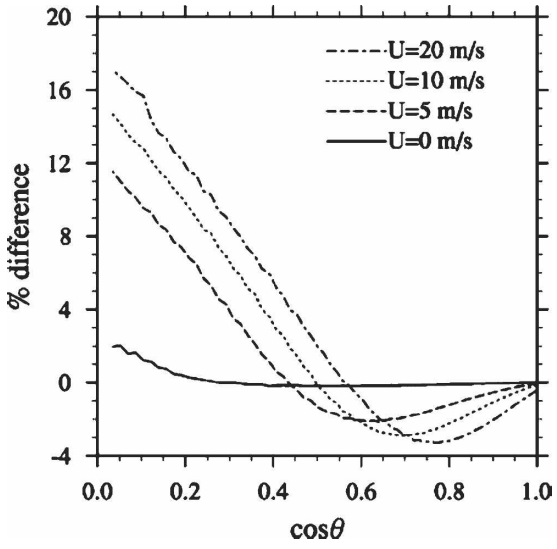

FIG. 4. Relative differences of solar irradiance reflectance in the 200–700-nm region between the wind-blown sea surface used in the COART and the results from the Monte Carlo simulation for cases of varying wind speeds (U = 0, 5, 10, and 20 m s^{-1}). Values >0 indicate that results from the Monte Carlo simulation have larger reflectance.

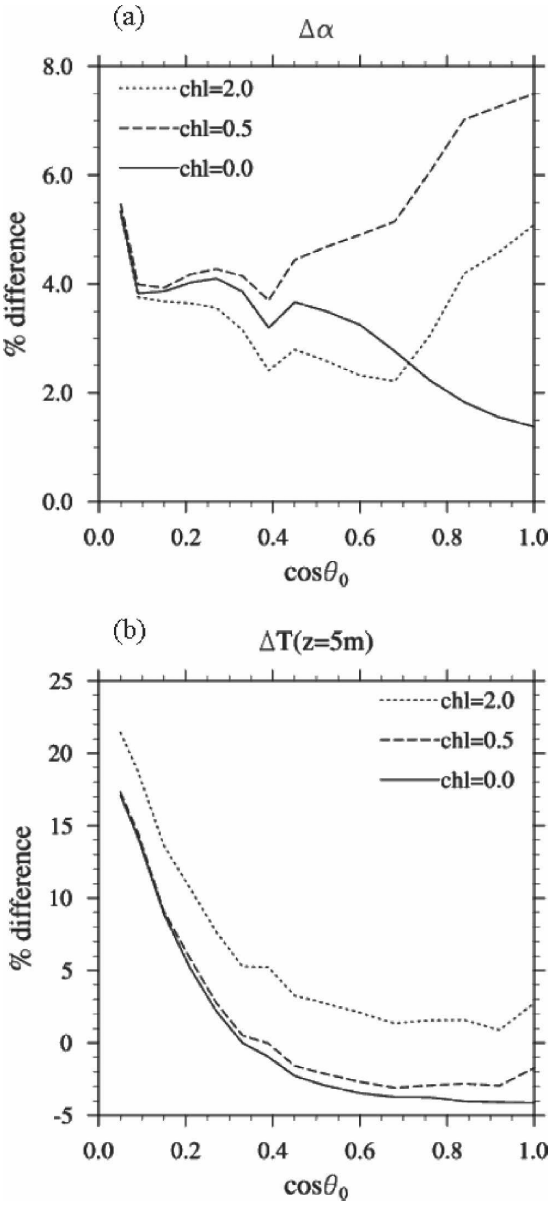

FIG. 5. Relative differences in (a) albedo and (b) transmission at z = 5 m with a flat sea surface for various chlorophyll concentrations between the results from the four-stream approximation and from COART. Values >0 indicate that the value calculated from the four-stream approximation is larger.

respectively. The additional streams in the ocean are to account for the region of total internal reflection. The COART also employed the Cox–Munk surface slope distribution to calculate the wind-blown sea surface reflectance and transmittance (Jin and Simpson 1999). However, the effects of multiple scattering and occultation (shadowing of one facet by another) are not taken into account in COART. Let R_c and R_m denote the irradiance reflectance of the COART sea surface and the reflectance from the full Monte Carlo simulation, respectively. Figure 4 shows the relative differences of reflectance defined as $\Delta R = (R_m - R_c)/R_c$ in the 200–700-nm region for different wind speed cases. Note that only Fresnel reflection is considered here. When $0.6 < \mu_0 < 0.8$, R_c is larger than R_m with the maximum difference by about 4%. For $\mu_0 < 0.4$, ΔR becomes negative due primarily to the neglect of multiple scattering in which the magnitude of ΔR is larger with higher wind speed. For a given SZA, the number of photons encountering multiple scattering generally increases with wind speed, resulting in an increase in surface reflectance. Similarly, a decrease in the sun's altitude also leads to an increase in the events of multiple scattering and surface reflectance.

To reduce the differences due to the treatment of atmospheric absorption and scattering, all model runs are for clear-sky conditions. For the first three solar bands used in the four-stream code (200–700, 700–1300, and 1300–1900 nm), the relative differences are generally less than 2%. Since 96% of solar flux lies in the first three bands, the downward fluxes at the sea surface in these two models are essentially the same. Let the albedo and transmission computed by COART be denoted by $\hat{\alpha}$ and $\hat{T}$, respectively. Then their relative differences are defined by $\Delta\alpha = (\alpha - \hat{\alpha})/\hat{\alpha} \times 100\%$ and $\Delta T = (T - \hat{T})/\hat{T} \times 100\%$. Model runs are performed for wind speeds from 0 to 18 m s^{-1} with an interval of 2 m s^{-1}, the cosines of SZA from 0.05 to 1 with an

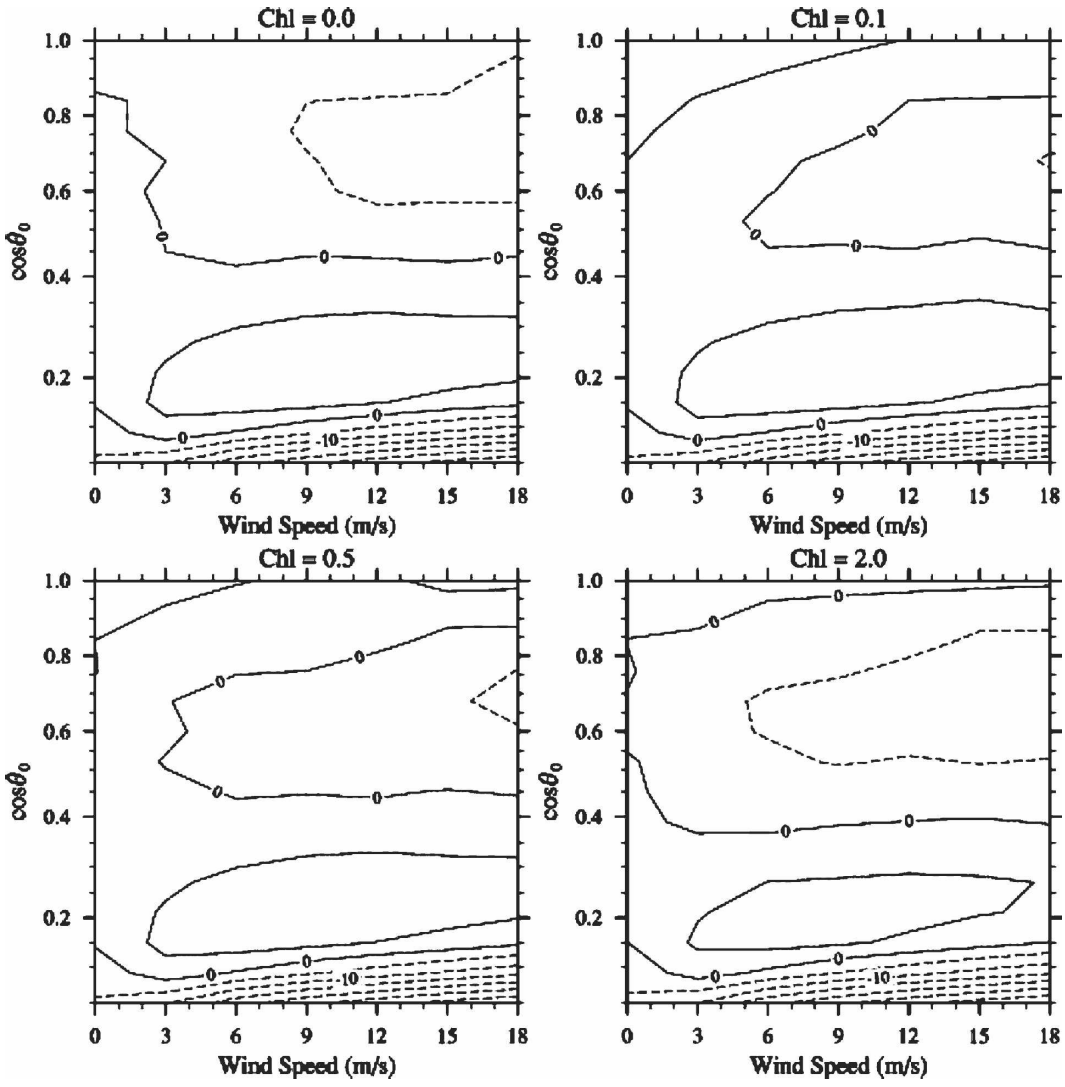

FIG. 6. As in Fig. 3 but for the relative difference of sea surface albedo $\Delta\alpha$ and chlorophyll concentrations of 0, 0.1, 0.5, and 2 mg m^{-3}. Contour interval is 5. Dashed lines indicate negative values.

interval of 0.05, and the chlorophyll concentrations (chl) of 0, 0.1, 0.5, and 2.0 mg m^{-3}.

Since the treatment of the sea surface roughness in the COART differs from our model, we first compare the calculated albedo and transmission using a flat sea surface. Figure 5 shows $\Delta\alpha$ and $\Delta T(z = 5\text{ m})$ with various chlorophyll concentrations as a function of SZA. For surface albedo, $\Delta\alpha$ are generally less than 5% for the cases involving chl = 0.0 and 2.0. Relative differences greater than 5% occur for the case of chl = 0.5 when $\mu_0 > 0.7$, showing a maximum of 7.5%. For the transmission at a depth equal to 5 m, large differences, on the order of 10%–20%, occur when $\mu_0 < 0.15$. It is noted that ΔT decreases significantly with SZA for $\mu_0 < 0.4$ but is less than 5% for the cases of chl = 0.0 and 0.5 when $\mu_0 > 0.2$ and for the case chl = 2.0 when $\mu_0 > 0.3$.

For wind-blown surface cases, the relative difference of the surface albedo for chlorophyll concentrations of 0, 0.1, 0.5, and 2.0 are shown in Fig. 6. Large differences on the order of 10%–30% for $\mu_0 < 0.1$ are shown and increase as wind speed increases. However, since only a small portion of solar energy can reach the sea surface when SZA is large, absolute differences in this region are very small. For the clear-sky condition in the Tropics, the corresponding radiative flux for a 10% difference with $\mu_0 = 0.1$ is 2.3 W m^{-2} (with reference to the surface net flux of 44 W m^{-2}) and that for a 25% difference with $\mu_0 = 0.05$ is 2.1 W m^{-2} (with reference to the net flux of 17 W m^{-2}). Differences larger than 5%

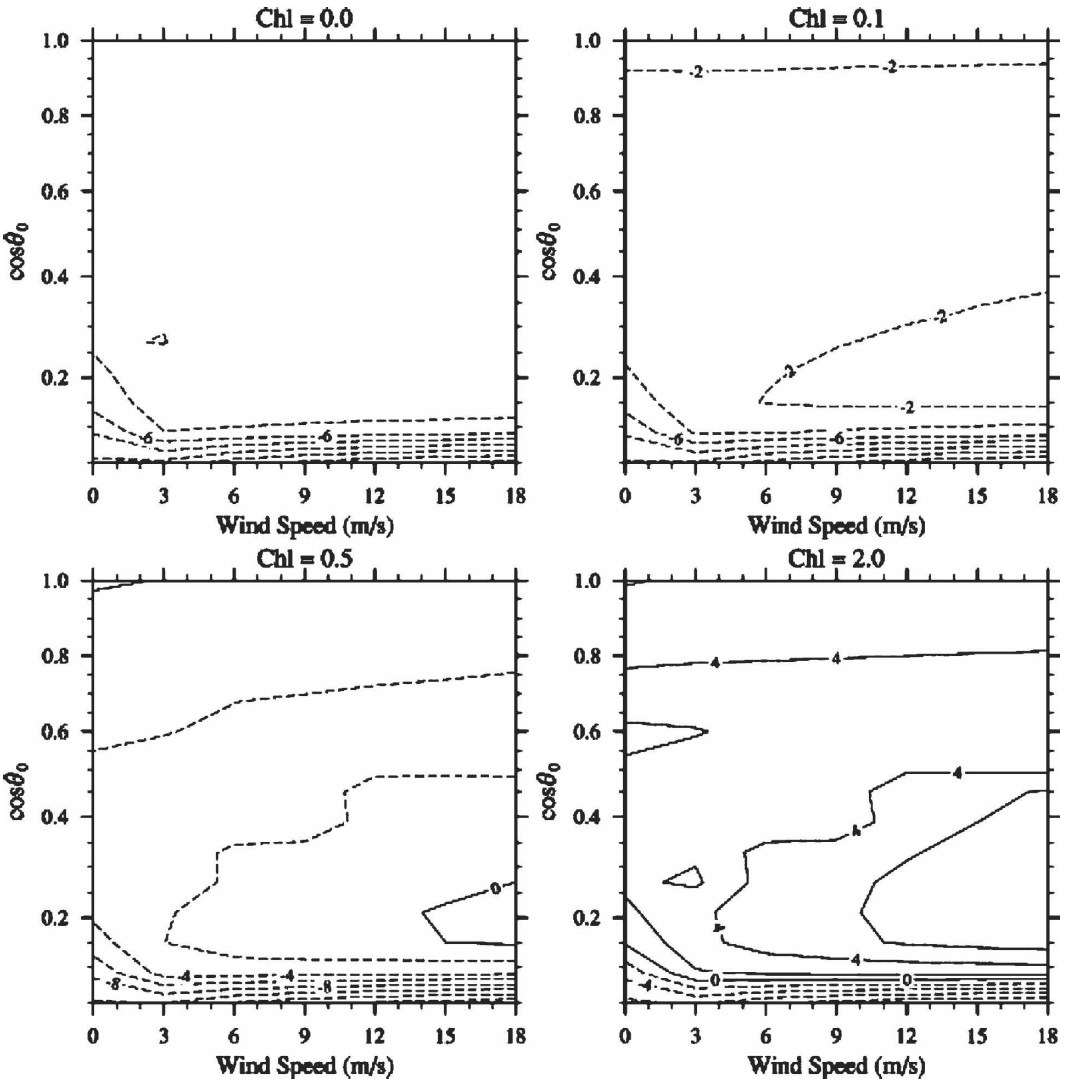

FIG. 7. As in Fig. 6 but for the relative difference in the total transmission ΔT at an ocean depth of 5 m. Contour interval is 2. Dashed lines indicate negative values.

also occur in the region of $0.15 < \mu_0 < 0.3$ with the wind speed larger than 3 m s^{-1} and $0.6 < \mu_0 < 0.8$ with the wind speed larger than 6 m s^{-1}. These two regions with large discrepancies correspond to differences in the irradiance reflectance between COART and our model, shown in Fig. 4. For the surface albedo calculation, the present model generally produces relative differences within about 5%.

Figure 7 shows the relative differences for the transmission at a depth of 5 m. Similar to the surface albedo case, differences in the total transmission larger than 6% occur for very large SZA ($\mu_0 < 0.1$). The absolute difference is also small. For example, the corresponding radiative flux of a 10% difference is 0.08 W m^{-2} for $\mu_0 = 0.1$ with a chlorophyll concentration of 0. The patterns of relative differences at other depths are similar to the results at the 5-m depth (results not shown). Relative differences are generally less than 10%, and discrepancies larger than 15% only occur when $\mu_0 < 0.15$.

4. Comparison to observation data

The COVE site is an ocean platform located 25 km off the coast of Virginia Beach near the mouth of the Chesapeake Bay. The elevation of the platform is 35 m above the sea surface, and the ocean is 11 m deep at this location. Radiation measurements at COVE included broadband downwelling and upwelling fluxes for both solar and thermal infrared radiation. Because the shadowing from the platform affects the reflected upward solar radiation, only the afternoon data were used in

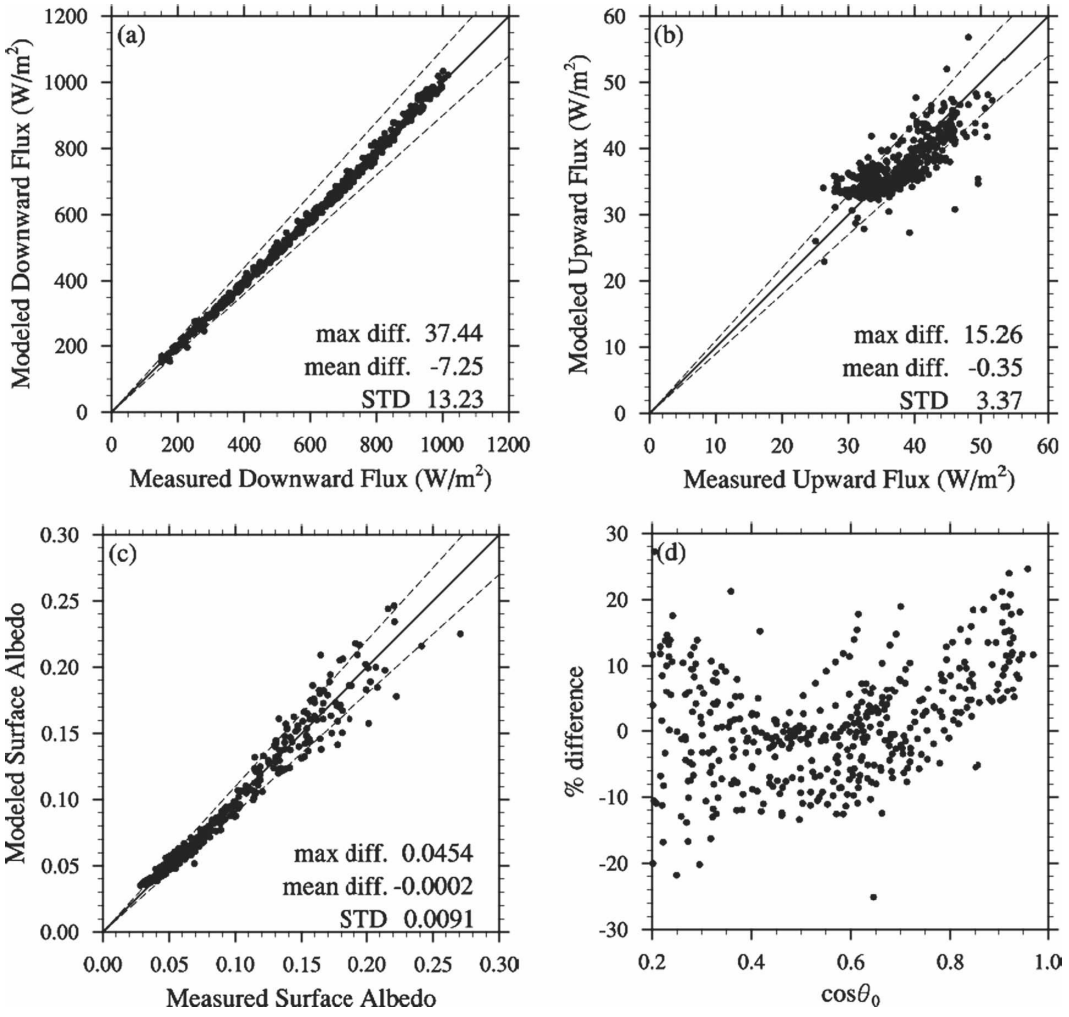

FIG. 8. Model–observation comparison for the broadband (a) downward and (b) upward shortwave flux and (c) surface albedo. Dashed lines indicate 10% relative difference. (d) Relative differences in surface albedo between model and observation (model − observation).

comparison. Aerosol optical depth, temperature, relative humidity, pressure, wind speed, wind direction, and cloud fraction are also measured at COVE. All observation data were averaged over a 15-min time period. Because the COVE site is close to the coast, we assume that the aerosol constituents are a combination of continental and maritime types with each contributing 50% of the aerosol optical depth. In this study, data collected in 2001 and 2002 were used for comparison. To reduce the uncertainty in cloud optical properties, only the data with zero cloud fraction were selected. Other necessary environmental variables, such as temperature, pressure, and water vapor profiles, total ozone burden, and chlorophyll concentration, were taken from the Moderate Resolution Imaging Spectroradiometer (MODIS)/*Terra* database.

Figure 8 shows a comparison of the total downward solar flux, the total upward flux, and albedo between model results and observations. The maximum absolute difference between the two, the mean difference, and the standard deviation are also shown in the figure. The model and observation display better agreement for the downward flux. Although the upward flux and surface albedo show larger variations, their relative differences are generally within 10%. The mean differences for both downward and upward flux are negative. Since the data is under clear-sky conditions, the discrepancy in downward flux may imply that the input aerosol type may be inaccurate, such that absorption due to aerosols is underestimated.

The relative differences in albedo are shown in Fig. 8d. Note that they are very scattered when $\mu_0 < 0.4$. It indicates that a small uncertainty in the environmental variables related to the surface roughness, such as wind

speed or wind direction, can result in a large difference of the surface albedo. We also find that, when $\mu_0 > 0.5$, the relative difference in albedo increases with μ_0. When the zenith angle of the downward incident ray is small, the Monte Carlo simulation reveals that reflectance can increase by 10% when the wind speed increases from 0 to 20 m s^{-1}. Thus, part of the error could be explained by uncertainty in wind speed. Because the COVE platform is higher than 12.5 m, the level at which the wind speed measurements were used for the construction of Cox–Munk surfaces, it is possible that the wind speed measured by the COVE site is too large for input to model calculations.

5. Conclusions

In this paper, we have presented a radiative transfer model based on the delta-four-stream approximation for the coupled atmosphere–ocean system. To calculate the reflection and refraction at a wind-blown sea surface and to account for the effect of multiple scattering, we employed the Monte Carlo model to simulate the photon traveling across the air–sea interface. The lookup table for surface reflectance and transmittance can then be constructed to implement the boundary conditions that are required in the four-stream approximation for radiative transfer. We compared the model results to the values produced by the COART radiative transfer program, which uses more radiative streams in the calculations. We show that the present efficient computational scheme can achieve relative differences within 5% for both surface albedo and total transmission at solar zenith angles less than 80°. Some large discrepancies between the two models are probably due to the difference in the treatment of surface roughness. We also compared our model results with observation data derived from the COVE experiment and found reasonable agreement. Relative differences in the downward and upward solar fluxes and albedo are generally within 10%. Our comparison results suggest that the aerosol type assumed and the measured wind speed used in model calculations could be the critical factors in producing differences in radiative flux comparison.

Finally it should be pointed out that the solutions of the four-stream approximation for radiative transfer are in analytic form, the computational effort is minimal, and at the same time the radiative flux can be obtained at arbitrary optical depth regardless of the vertical grid. Because it is computationally efficient while maintaining excellent accuracy, this model is well suited for incorporation in a coupled atmosphere–ocean global circulation model for consistent flux and heating rate calculations in the atmosphere and ocean mixed layer.

Acknowledgments. The research of this work has been supported in part by NSF Grant ATM-0331550 and DOE Grant DE-FG03-00ER62904. We thank Dr. Z. Jin for providing the online version of the COART model for intercomparison.

REFERENCES

Born, M., and E. Wolf, 1980: *Principles of Optics: Electromagnetic Theory of Propagation, Interference and Diffraction of Light.* 6th ed. Pergamon Press, 808 pp.

Chandrasekhar, S., 1950: *Radiative Transfer*. Clarendon Press, 393 pp.

Cox, C., and W. Munk, 1954: Measurement of the roughness of the sea surface from photographs of the sun's glitter. *J. Opt. Soc. Amer.,* **44,** 838–850.

Frouin, R., M. Schwindling, and P.-Y. Deschamps, 1996: Spectral reflectance of sea foam in the visible and near-infrared: In situ measurements and remote sensing implications. *J. Geophys. Res.,* **101,** 14 361–14 371.

Fu, Q., and K. N. Liou, 1992: On the correlated *k*-distribution method for radiative transfer in nonhomogenecous atmospheres. *J. Atmos. Sci.,* **49,** 2139–2156.

——, and ——, 1993: Parameterization of the radiative properties of cirrus clouds. *J. Atmos. Sci.,* **50,** 2008–2025.

Gordon, H. R., and A. Morel, 1983: *Remote Assessment of Ocean Color for Interpretation of Satellite Visible Imagery: A Review*. Spring-Verlag, 114 pp.

——, O. B. Brown, R. H. Evans, J. W. Brown, R. C. Smith, K. S. Baker, and D. K. Clark, 1988: A semianalytic radiance model of ocean color. *J. Geophys. Res.,* **93,** 10 909–10 924.

Gu, Y., J. Farrara, K. N. Liou, and C. R. Mechoso, 2003: Parameterization of cloud–radiation processes in the UCLA general circulation model. *J. Climate,* **16,** 3357–3370.

Hale, G. M., and M. R. Querry, 1973: Optical constants of water in the 200-nm to 200-μm wavelength region. *Appl. Opt.,* **12,** 555–563.

Jin, Z., and K. Stamnes, 1994: Radiative transfer in nonuniformly refracting layered media: Atmosphere-ocean system. *Appl. Opt.,* **33,** 431–442.

——, and J. J. Simpson, 1999: Bidirectional anisotropic reflectance of snow and sea ice in AVHRR channel 1 and 2 spectral regions. Part I: Theoretical analysis. *IEEE Trans. Geosci. Remote Sens.,* **37,** 543–554.

——, T. P. Charlock, and K. Rutledge, 2002: Analysis of broadband solar radiation and albedo over the ocean surface at COVE. *J. Atmos. Oceanic Technol.,* **19,** 1585–1601.

Liou, K.-N., 1974: Analytic two-stream and four-stream solutions for radiative transfer. *J. Atmos. Sci.,* **31,** 1473–1475.

——, 2002: *An Introduction to Atmospheric Radiation*. 2d ed. Academic Press, 583 pp.

——, Q. Fu, and T. P. Ackerman, 1988: A simple formulation of the delta-four-stream approximation for radiative transfer parameterizations. *J. Atmos. Sci.,* **45,** 1940–1948.

Mobley, C. D., 1994: *Light and Water: Radiative Transfer in Natural Waters*. Academic Press, 592 pp.

Moore, K. D., K. J. Voss, and H. R. Gordon, 2000: Spectral reflectance of whitecaps: Their contribution to water-leaving radiance. *J. Geophys. Res.,* **105,** 6493–6499.

Morel, A., 1988: Optical modeling of the upper ocean in relation to its biogenous matter content (case I waters). *J. Geophys. Res.,* **93,** 10 749–10 768.

——, 1991: Light and marine photosynthesis: A spectral model with geochemical and climatological implications. *Prog. Oceanogr.,* **26,** 263–306.

——, and L. Prieur, 1977: Analysis of variations of ocean color. *Limnol. Oceanogr.,* **22,** 709–772.

——, and S. Maritorena, 2001: Bio-optical properties of oceanic waters: A reappraisal. *J. Geophys. Res.,* **106,** 7163–7180.

Ohlmann, J. C., D. A. Siegel, and C. Gautier, 1996: Ocean mixed layer radiant heating and solar penetration: A global analysis. *J. Climate,* **9,** 2265–2280.

Petzold, T. J., 1972: Volume scattering functions for selected ocean waters. Scripps Institution of Oceanography Visibility Laboratory Tech. Rep. 72–78, 79 pp.

Preisendorfer, R. W., and C. D. Mobley, 1985: Unpolarized irradiance reflectances and glitter patterns of random capillary waves on lakes and seas, by Monte Carlo simulation. NOAA/ Pacific Marine Environmental Laboratory Tech. Memo. 63, 141 pp.

Prieur, L., and S. Sathyendranath, 1981: An optical classification of coastal and oceanic waters based on the specific spectral absorption curves of phytoplankton pigments, dissolved organic matters, and other particulate materials. *Limnol. Oceanogr.,* **26,** 671–689.

Siegel, D. A., J. C. Ohlmann, L. Washburn, R. R. Bidigare, C. Nosse, E. Field, and Y. Zhou, 1995: Solar radiation, phytoplankton pigments, and radiant heating of the equatorial Pacific warm pool. *J. Geophys. Res.,* **100,** 4885–4891.

Smith, R. C., and K. S. Baker, 1981: Optical properties of the clearest natural waters (200–800 nm). *Appl. Opt.,* **20,** 177–184.

Sykes, J. B., 1951: Approximation integration of the equation of transfer. *Mon. Not. Roy. Astron. Soc.,* **111,** 377–386.